Development and Validation of Flat-Plate Collector Testing Procedures

Report for January, 2007

Focus on Energy (FOE) supports solar thermal systems that displace conventional fuels by offering cash-back rebates that provide an incentive for residents to invest in this renewable energy technology. To be eligible for rebates, FOE requires solar collectors to be certified by the Solar Rating and Certification Corporation (SRCC). The certification program involves testing of the solar collectors in accordance with ASHRAE Standard 93-2003[1]. Currently, these tests are only provided in Florida (outdoors) by the Florida Solar Energy Center (FSEC).

Wisconsin's flat plate collector testing program will be done at Madison Area Technical College (MATC). The UW-Solar Energy Laboratory is assisting MATC personnel in establishing a suitable implementation of the ASHRAE test method. The UW further intends to identify alternative test methods that can be done indoors or under conditions that are more suitable to Wisconsin weather, but still provide the information required by the ASHRAE 93-2003 test. What follows is the fourth report of this activity.

Table of contents

1. Data analysis thermal efficiency test (TestAnalyzer.m)

The thermal efficiency test has been described in Report 2 (November 2006). To analyze the test data the software TestAnalyzer has been developed. TestAnalyzer generates a test report based on the test data production files. The first section of this report describes how the actual version software works.

17 test days have been performed at MATC in October, November, and December 2006. TestAnalyzer has been used to analyze the test data produced during these tests. The first results of the analysis are presented in the second section of this report.

1.1. Overview

The test data are analyzed in four steps which are visualized in Figure 1. First the production file generated during the collector tests is prepared for the analysis. The module *MeanMatrix.m* determines all required values and adds external data. The result of this step is the matrix '*meanmatrix*'. During the second step the module *TCC.m* identifies valid data points within *meanmatrix*. This is done by performing test condition checks based on the test conditions defined in the ASHRAE Standard 93-2003. The result of the second step is a matrix '*datapoints*' which contains all valid data points for the test day. During the third step the efficiencies for the data points are calculated and saved in the matrix '*results*'. The last step generates a report which contains all required data and plots including the efficiency curve of the collector. All steps and the related program modules are described below.

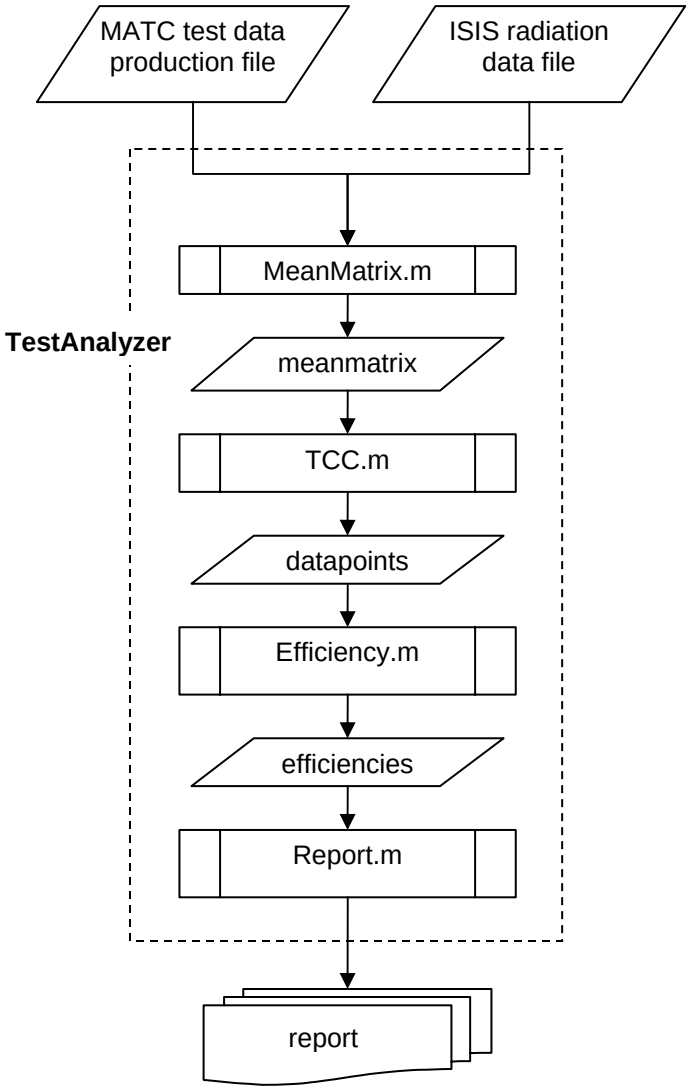

Figure 1 TestAnalyzer data analysis process

1.2. Generation of the mean matrix (*MeanMatrix.m*)

Before the procedure of test condition check and efficiency calculation begins, all required variables are calculated and saved in the matrix '*meanmatrix*'.

1.2.1. Average values

TestAnalyzer allows averaging the values in the original test data file. This is done by setting the parameter '*interval'* to the number of rows for which one average value should be calculated. In the following this interval is called 'average interval'. It is important to mention that this interval is not a time interval but a number of measurements or rows in the test data file. If the parameter *interval* is set to 10, for each 10 measurements one average value in meanmatrix is generated. This method works only for measurements which are taken in approximately equal time steps.

1.2.2. Time

The time reported in the generated matrix *meanmatrix* is the time of day in seconds at the *end* of each average interval. The time is saved in the first column of *meanmatrix*.

To simplify further calculations the length of the average interval in seconds is calculated and reported in the second column. This is important for data files where the measurements are not taken over exactly constant time intervals. If measurements were taken in constant intervals, this column should contain equal values in every row.

1.2.3. Gallons counter

The value of the gallons counter at the end of each average interval is saved in the third column of *meanmatrix*.

The increase of the gallons counter during the average interval is saved in the fourth column of *meanmatrix*.

1.2.4. Temperatures, pressures, solar irradiance, wind speed

Columns 5 through 11 are filled with the average values of inlet, outlet and ambient temperature, inlet and outlet pressure, solar irradiance, and wind speed.

1.2.5. Volume flow rate

The volume flow rate is calculated by dividing the increase in gallons (column 2 of *meanmatrix*) by the increase in seconds (column 4 of *meanmatrix*). The result is divided by 60 to obtain a value in gallons per minute and saved in column 12 of *meanmatrix*.

1.2.6. Mass flow rate

The volume flow rate value is converted to liters per second, multiplied with the density of the heat transfer fluid, and saved in column 13 of *meanmatrix*. The density is determined in a separate module '*Density.m*' described in chapter 1.3 of this report.

1.2.7. Specific heat

The specific heat of the heat transfer fluid is calculated in a separate module '*SpecHeat.m*' described in chapter 1.4 of this report. It is saved in column 14 of *meanmatrix*.

The ASHRAE Standard 93-2003 mentions the temperature dependence of the specific heat in chapter 5.1.3, but does not specify which temperature shall be used for the calculation of the specific heat. For the analysis in *MeanMatrix.m* the mean values of the collector inlet and outlet temperatures (the mean fluid temperature) are used.

1.2.8. Useful energy gain and incident solar energy

At this point the useful energy gain and the incident solar energy for the average interval are calculated based on the values already contained in *meanmatrix* and saved in columns 15 and 16, respectively. The useful energy gain is the product of the time interval (2), the mass flow rate (13), the difference between inlet temperature (5) and outlet temperature (6) and the specific heat (14). The incident solar radiation is the product of the time

interval (2) and the solar irradiance (10). The numbers in brackets are the related columns of *meanmatrix*.

1.2.9. Instantaneous thermal efficiency

The ratio of useful energy gain and incident solar energy is a measure of the instantaneous thermal efficiency of the collector during the average interval. It is saved in column 17 of *meanmatrix*.

1.2.10. Incident angle and solar time

The incident angle and solar time are calculated in a separate module '*IncidentAngle.m*', based on the local time and the collector orientation, and saved in columns 18 and 19, respectively. This information is important for tests with a fixed mount in order to check whether the incident angle is within the allowed range and whether the data points are symmetric to solar noon.

1.2.11. ISIS data

As only one pyranometer is installed at the MATC test facility, only total solar irradiance is measured. Additionally solar beam radiation measurements are required by the test method. The required data are obtained from ISIS[1] radiation measurements in Madison. The following variables are added to *meanmatrix* (column numbers in brackets): total solar radiation on a horizontal surface (20), beam radiation normal to sun (21), diffuse radiation (22), and solar zenith angle (23). A separate module '*ISISread.m*' is used for extracting the values from the ISIS data files. The module is described in Chapter 1.6 of this report.

1.2.12. Total solar irradiance normal to sun

The total solar irradiance normal to sun is calculated with the module *TotalNormal.m* described in chapter 1.7 and saved in column 24 of *meanmatrix*.

1.2.13. Diffuse irradiance upon collector plane

The diffuse irradiance upon the collector plane G_d is calculated with the following equation (ASHRAE 93-2003, Equation (8.19)):

$$G_d = G_t - G_{DN} \cdot \cos(\theta) \tag{1.1}$$

where G_t is the total irradiance upon the collector plane (*meanmatrix* column 10), G_{DN} is the beam radiation normal to sun (*meanmatrix* column 21) and θ is the incidence angle of the beam radiation with respect to the normal of the collector plane (*meanmatrix* column 18) and saved in column 25 of *meanmatrix*.

1.2.14. Diffuse irradiance fraction upon collector plane

The diffuse irradiance fraction upon the collector plane is the diffuse irradiance upon the collector plane (*meanmatrix* column 25) divided by the total irradiance upon the collector

[1] Integrated Surface Irradiance Study (ISIS) Network, http://www.srrb.noaa.gov/isis/index.html

plane (*meanmatrix* column 10). To obtain values in % the result is multiplied with 100. It is saved in column 26 of *meanmatrix*.

1.2.15. Wind direction

The mean value of the wind direction is calculated from the test data file and saved in column 27 of *meanmatrix*.

1.2.16. Summary

Table 1 summarizes all variables saved in the mean matrix.

Table 1 Structure of mean matrix

Column	Variable	Units
1	Time of day	sec
2	Length of average interval	sec
3	Gallons counter	gal
4	Increase of gallons counter[1)]	gal
5	Collector inlet temperature	°F
6	Collector outlet temperature	°F
7	Ambient temperature	°F
8	Collector inlet pressure	PSI
9	Collector outlet pressure	PSI
10	Solar irradiance	W/m^2
11	Wind speed	m/s
12	Volume flow rate	gpm
13	Mass flow rate	kg/s
14	Specific heat of heat transfer fluid	kJ/kg-K
15	Useful energy gain[1)]	kJ
16	Incident solar energy[1)]	kJ
17	Instantaneous thermal efficiency[1)]	-
18	Incident angle at the end of average interval	deg
19	Solar time at the end of average interval	sec
20	Total radiation on horizontal surface (ISIS)	W/m^2
21	Beam radiation normal to sun (ISIS)	W/m^2
22	Diffuse radiation on horizontal surface (ISIS)	W/m^2
23	Solar zenith angle (ISIS)	deg
24	Total solar irradiance normal to sun	W/m^2
25	Diffuse radiation upon collector plane	W/m^2
26	Diffuse fraction	%
27	Wind direction	deg

[1)] during average interval

1.3. Determination of the fluid density (Density.m)

In order to calculate the mass flow rate through collector from the measured volume flow rate, the determination of the fluid density is required. Generally the density of a fluid depends on its pressure and temperature. This chapter evaluates the relevance of these dependencies for the analysis of the test data and derives a calculation method for the fluid density.

The test setup used at MATC is an open system. Fluid pressures are measured at collector inlet and outlet. The heated water leaving the collector is dumped to the surroundings. Tests have shown that the measured gauge pressure values vary between -2 and 5 PSI. The fluid temperature ranges between 3 and 96°C.

The pressure dependence of the density of water has been calculated for four temperatures using EES[2]. The results are shown in Table 2. These results show that there is no change in density over the relevant pressure range for a constant temperature. Consequently the density determination used in Density.m is not based on the measured pressure but on a pressure of one atmosphere throughout all the test data analysis. This approximation simplifies the analysis without reducing the quality of the results. Of course, the assumption of pressure independence is only valid if the water remains liquid. Otherwise a significant change in density occurs. So during the test the outlet pressure should be maintained above zero gauge pressure as soon as the outlet temperature exceeds a value of 95°C.

Table 2 Pressure dependency of the density of water

P_gauge [PSI]	P_gauge_kPa [kPa]	P_abs [kPa]	Density 3°C [kg/m^3]	Density 30°C [kg/m^3]	Density 60°C [kg/m^3]	Density 90°C [kg/m^3]
-2.0	-13.8	87.5	1000	995.6	983.2	965.3
-1.5	-10.3	91.0	1000	995.6	983.2	965.3
-1.0	-6.9	94.4	1000	995.7	983.2	965.3
-0.5	-3.4	97.9	1000	995.7	983.2	965.3
0.0	0.0	101.3	1000	995.7	983.2	965.3
0.5	3.4	104.8	1000	995.7	983.2	965.3
1.0	6.9	108.2	1000	995.7	983.2	965.3
1.5	10.3	111.7	1000	995.7	983.2	965.4
2.0	13.8	115.1	1000	995.7	983.2	965.4
2.5	17.2	118.6	1000	995.7	983.2	965.4
3.0	20.7	122.0	1000	995.7	983.2	965.4
3.5	24.1	125.5	1000	995.7	983.2	965.4
4.0	27.6	128.9	1000	995.7	983.2	965.4
4.5	31.0	132.4	1000	995.7	983.2	965.4
5.0	34.5	135.8	1000	995.7	983.2	965.4

If the test setup is changed to a closed loop system the fluid can be pressurized. For the new situation with possibly increased pressure values compared to those observed during the open loop tests the considerations for pressure dependence must not be repeated. Table 3 shows the density for pressures up to 1000 kPa.

[2] Engineering Equation Solver, http://www.fchart.com/

Table 3 Pressure dependence of the density of water for pressurized system

P_abs	Density 3°C	Density 30°C	Density 60°C	Density 60°C
[kPa]	[kg/m^3]	[kg/m^3]	[kg/m^3]	[kg/m^3]
100	1000	995.7	983.2	965.3
200	1000	995.7	983.2	965.4
500	1000	995.7	983.3	965.4
600	1000	995.8	983.3	965.5
700	1000	995.8	983.4	965.5
800	1000	995.9	983.4	965.6
900	1000	995.9	983.5	965.6
1000	1000	996	983.5	965.7

The relevant temperature for the density determination is the collector inlet temperature, as the volume flow rate is measured at the collector inlet. The density of water has been calculated for a temperature range from 1 to 100°C using EES. The results are presented in Table 4. It is obvious that the density of water depends significantly on the temperature over the given range. Consequently *Density.m* determines the density with respect to the collector inlet temperature.

Table 4 Temperature dependence of the density of water calculated with EES

T [C]	Density [kg/m^3]
0.00	916.7
10.00	999.7
20.00	998.2
30.00	995.7
40.00	992.2
50.00	988.0
60.00	983.2
70.00	977.8
80.00	971.8
90.00	965.3
100.00	958.4

1.4. Determination of the specific heat (SpecHeat.m)

The specific heat of a fluid generally depends on temperature and pressure. This section describes how the specific heat for water is handled during the analysis process.

The test setup used at MATC is an open system. Pressures are measured at collector inlet and outlet. The heated water is dumped to the surroundings. Tests have shown that the measured gauge pressure values vary between -2 and 5 PSI. The fluid temperature range is 3 to 96°C.

The pressure dependence of the specific heat of water has been calculated for four temperatures using EES. The results are shown in Table 5. These results show that there is no change in specific heat over the relevant pressure range. Consequently the heat capacity calculations are based on a pressure of one atmosphere in SpecHeat.m, just as for density. Of course, the assumption of pressure independence is only valid if the water remains liquid. So during the test the outlet pressure should be maintained above zero gauge pressure as soon as the outlet temperature exceeds a value of 95°C. Furthermore, if the test setup is changed to a closed loop system the fluid can be pressurized. For the new situation with possibly increased pressure values compared to those observed during the open loop tests the considerations for pressure dependence must be repeated and the module SpechHeat.m must be adapted if required.

Table 5 Pressure dependence of the specific heat of water at 3°C, 30°C, 60°C, 90°C and 1 atm calculated with EES

P_gauge [PSI]	P_gauge [kPa]	P_abs [kPa]	cp 3°C [kJ/kg-K]	cp 30°C [kJ/kg-K]	cp 60°C [kJ/kg-K]	cp 90°C [kJ/kg-K]
-2	-13.79	87.54	4.208	4.183	4.183	4.204
-1.5	-10.34	90.98	4.208	4.183	4.183	4.204
-1	-6.895	94.43	4.208	4.183	4.183	4.204
-0.5	-3.447	97.88	4.208	4.183	4.183	4.204
0	0	101.3	4.208	4.183	4.183	4.204
0.5	3.447	104.8	4.208	4.183	4.183	4.204
1	6.895	108.2	4.208	4.183	4.183	4.204
1.5	10.34	111.7	4.208	4.183	4.183	4.204
2	13.79	115.1	4.208	4.183	4.183	4.204
2.5	17.24	118.6	4.208	4.183	4.183	4.204
3	20.68	122	4.208	4.183	4.183	4.204
3.5	24.13	125.5	4.208	4.183	4.183	4.204
4	27.58	128.9	4.208	4.183	4.183	4.204
4.5	31.03	132.4	4.208	4.183	4.183	4.204
5	34.47	135.8	4.208	4.183	4.183	4.204

The specific heat of water has been calculated for a temperature range from 1 to 100°C using EES. The results are presented in Table 6. *SpechHeat.m* determines the specific heat with respect to the temperature provided as parameter.

Table 6 Temperature dependence of the specific heat capacity of water calculated with EES

T [C]	cp [kJ/kg-K]
1	4.220552
2	4.213989
3	4.208404
4	4.203662
5	4.199662
6	4.196309
7	4.193517
8	4.191209
9	4.189328
10	4.187790
20	4.183002
30	4.183082
40	4.182219
50	4.181468
60	4.182649
70	4.186788
80	4.194101
90	4.204328
100	4.217072

1.5. Determination of incident angle and solar time (IncidentAngle.m)

The module *IncidentAngle.m* returns the incident angle on a tilted surface and the solar time for the following parameters (definitions taken from Duffie, Beckman (2006)):

Table 7 Parameters of the module IncidentAngle.m

n	nth day of the year (1 ... 365)
phi	Latitude, the angular location north or south of the equator, north positive; -90°<=phi<=90°
beta	Slope, the angle between the plane of the surface in question and the horizontal; 0°<=beta<=180° (beta>90° means that the surface has a downward-facing component.
gamma	Surface azimuth angle, the deviation of the projection on a horizontal plane of the normal to the surface from the local meridian, with zero due south, east negative, and west positive; -180° <= gamma <=180°
localtime	local time in seconds
daylightsaving	1 if localtime is daylight saving time and 0 if localtime is no daylight saving time
L_st	Standard meridian for local time zone
L_loc	Longitude of the location, in degress west; 0°<L_loc<360°

The following calculations are performed (all equations taken from Duffie, Beckman (2006)) to return the incidence angle and solar time:

```
B=(n-1)*(360/365);   %Degree per day - SETP(1.4.2)
E=229.2*(0.000075+0.001868*cosd(B)-0.032077*sind(B)-
0.014615*cosd(2*B)-0.04089*sind(2*B));  %Equation of time -
SETP(1.5.3)
standardtime=localtime-daylightsaving*3600;  %Local time is given in
seconds, 1 hour = 3600 sec must be subtracted during DST
solartime=standardtime+(4*(L_st-L_loc)+ E)*60;   %Solar time =
standard time + difference in minutes * 60 - SETP(1.5.2)
omega=15*(solartime/3600-12); %Hour angle, the angular displacement
of the sun east or west of the local meridian due to rotation of the
earth on its axis at 15° per hour; morning negative, afternoon
positive.
delta=0.006918-0.399912*cosd(B)+0.070257*sind(B)-
0.006758*cosd(2*B)+0.000907*sind(2*B)-
0.002679*cosd(3*B)+0.00148*sind(3*B);    %Declination equation from
Spencer(1971) - SETP(1.61b)
theta=acosd(sind(delta)*sind(phi)*cosd(beta)-
sind(delta)*cosd(phi)*sind(beta)*cosd(gamma)+cosd(delta)*cosd(phi)*co
sd(beta)*cosd(omega)+cosd(delta)*sind(phi)*sind(beta)*cosd(gamma)*cos
d(omega)+cosd(delta)*sind(beta)*sind(gamma)*sind(omega));
%Equation for the angle of incidence - SETP(1.6.2)
```

Figure 2 Matlab code of IncidentAngle.m

1.6. Reading ISIS radiation data (ISISread.m)

ISISread.m returns the following values for a given year, day of year, location and the time of day in seconds in Universal Coordinated Time (UTC):

total	Total radiation on a horizontal surface in W/m^2
beam	Beam radiation normal to sun in W/m^2
diffuse	Diffuse radiation on a horizontal surface in W/m^2
zenith	Solar zenith angle in degree

ISISread searches for the proper data file in the ISIS data directory, loads the file using the module ISISimport.m (Chapter 1.7), goes through the rows of the loaded ISIS data file until the time given as parameter is within the 3-minute interval of the actual row. Then the data listed above are read from this row and returned to the calling instance. The following columns in the ISIS data file are relevant:

Table 8 Structure of ISIS data files

Column number	Variable
7	Time of day as decimal number
8	Solar zenith angle
9	Total radiation (horizontal)
11	Beam radiation (normal)
13	Diffuse radiation (horizontal)

1.7. Importing ISIS radiation data files (ISISimport.m)

*ISISimport.*m imports the ISIS data file for the given year, day and location and loads the contained data into a structure array containing two matrices. The matrix *data* contains the measurements while the matrix *textdata* contains the two header lines. The matrices can be accessed as follows (example for year 2006, day 300, and location Madison):

```
A=ISISimport(2006,300,'msn')
B=A.data
C=A.textdata
```

The data files are provided by ISIS in the following ftp directory:

ftp://ftp.srrb.noaa.gov/pub/data/isis/

A local mirror of the ftp directory has been created; the path of the local directory must be defined within the *ISISimport.m* code.

1.8. Total solar irradiance normal to sun (TotalNormal.m)

At the MATC test facility only one pyranometer is installed to measure the total solar irradiance upon the collector plane. From this information alone the total solar irradiance normal to the sun can not be determined, as required in the test standard. This is why values for the irradiance normal to the sun are derived from ISIS data. The total solar irradiance on a horizontal plane I, the total diffuse radiation on a horizontal plane I_d and the beam radiation normal to the sun I_{bn} are measured and published as data files for each day of the year. These measurements are taken on top of the Engineering Research Building in Madison, which is about 5 miles from the MATC test site. Based on these measurements, the Liu and Jordan method is used to calculate the total solar irradiance normal to the sun I_n (Equation (1.2)):

$$I_n = I_{bn} + I_d\left(\frac{1+\cos(\beta)}{2}\right) + I\rho\left(\frac{1-\cos(\beta)}{2}\right) \qquad (1.2)$$

Figure 3 shows that the tilt angle β is always equal to the solar zenith angle θ_z, so β is given by Equation (1.3).

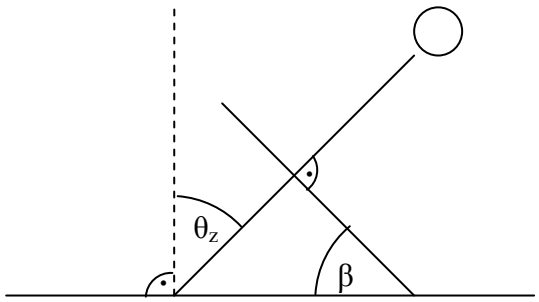

Figure 3 Tilt angle of a surface orientated normal to beam radiation

$$\beta = \theta_z \tag{1.3}$$

The ground reflectance must be determined at the test site. The ground reflectance is not constant throughout the year. A snow cover on the ground increases the ground reflectance significantly. As long as the ground reflectance is not known, a value of 0.3 is used as a reasonable value.

All three required radiation variables I_{bn}, I_d, and I are provided by ISIS. However, the three variables are dependent through Equations (1.4) and (1.5).

$$I_b = I_{bn} \cos(\beta) \tag{1.4}$$

$$I_d = I - I_b \tag{1.5}$$

As the beam and diffuse radiation measurements are typically of higher accuracy, the total radiation values are calculated from the beam and diffuse radiation measurements by using Equations (1.4) and (1.5). A separate chapter in one of the next reports will deal with the quality of total radiation measurements and discuss this issue in more detail.

The ISIS data is reported in average values over 3-minute-intervals. This means that a case as shown in Figure 4 can occur. While the mean value reported by ISIS is greater than the required lower limit, the actual total irradiance falls below the lower limit within the considered interval. If one were using the actual data instead of the three minute average values the sudden irradiance drop would cause a failure in the hard condition check. However, as the ASHRAE 93-2003 standard does prescribe the time intervals for calculating average values or taking measurements, the 3-minute ISIS data is used for the hard condition check and the possibility of a situation such as shown in Figure 4 is accepted. Still the data from the MATC pyranometer, which measures the irradiance every second, is used to check for soft conditions. So steady state behavior, as defined in ASHRAE Standard 93-2003, is guaranteed.

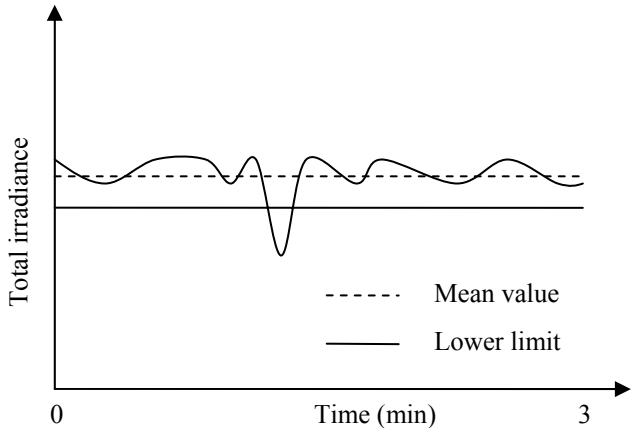

Figure 4 3-minutes-mean value and check for lower limits

1.9. Test conditions check (TCC.m)

1.9.1. Test periods and test conditions

In order to calculate the efficiencies, valid test periods within the test data must be identified. A test period contains a pre-data period and a data period as shown in Figure 1 of Report 2 (November 2006). A test period is valid if all requirements for the test conditions defined in the ASHRAE Standard 93-2003 are met. Test conditions have been described in Section 3 of Report 2 (November 2006), all of the following considerations refer to that section.

For the processing of the data, it is convenient to distinguish between two groups of test conditions. The first group contains the *hard conditions*. Hard conditions define absolute limits for a variable. Four hard test conditions for the thermal efficiency test are defined in the ASHRAE 93-2003 Standard and presented in Table 9.

Table 9 Hard conditions

Variable	**Steady State Condition** (Maximum/Minimum values)
Total solar irradiance normal to sun	Minimum 790 W/m^2
Fraction of diffuse radiation	Maximum 20%
Wind speed	Minimum 2.2 m/s
Wind speed	Maximum 4.5 m/s

The second group of test conditions contains *soft conditions*. Soft conditions define the maximum allowed range of a variable. Four soft conditions for the thermal efficiency test are defined in the ASHRAE 93-2003 Standard and presented in Table 10.

Table 10 Soft conditions

Variable	**Steady State Condition** (Maximum variation)
Total solar irradiance upon aperture plane	±32 W/m^2
Ambient temperature	±1.5 °C
Volume flow rate	±2 % or ±0.005 gpm[1)]
Inlet temperature	±2 % or ±1 °C[1)]

[1)] The *greater* one of both listed variations must be applied

TCC.m first checks a measurement for hard conditions and then for soft conditions. The process is visualized in Figure 5. If a measurement meets all test conditions, it is put into

the test period array and TCC proceeds with the next measurement. If the required amount of valid measurements has been collected, the row indices in *meanmatrix* of the data in the test period array are stored in the matrix '*datapoints'*. So *datapoints* does not contain the test data itself, but pointers to the valid dat apoints in *meanmatrix*. Table 11 shows the contents of the matrix *datapoints*.

Table 11 Variables in matrix datapoints

Column no	Variable	Units
1	Pre-data period start	row in meanmatrix
2	Data period start	row in meanmatrix
3	Test period end	row in meanmatrix

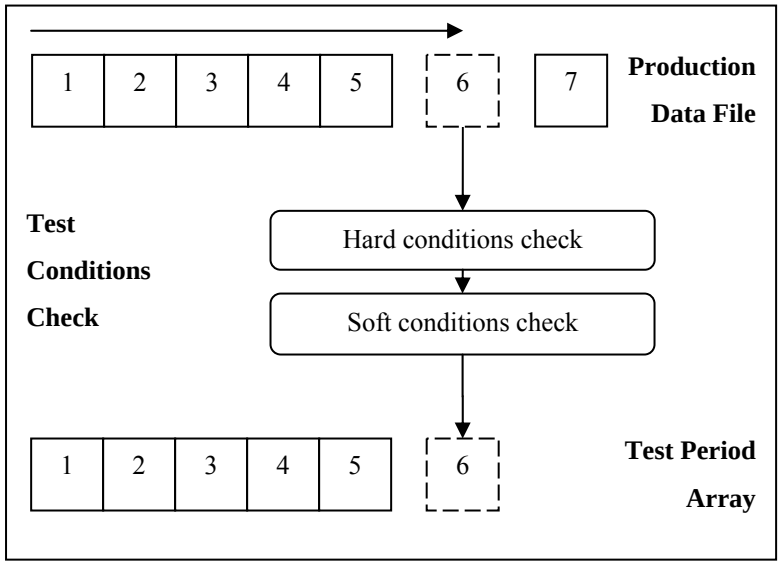

Figure 5 Data analysis: test conditions check, every number represents a single measurement

A distinction between hard and soft conditions has been introduced. This distinction is directly reflected in the way TCC handles these conditions. To check for the *hard conditions*, *TCC*.m compares the values of the measurements with the limits listed in Table 9. If a measurement does not meet all the hard conditions, the test period array is emptied, as it does not contain enough valid measurements for a complete test period. So if the hard conditions check is not passed all proceeding measurements for the actual test period are lost.

To check for the *soft conditions*, TCC calculates the mean value from all measurements in the test period array (measurements 1 to 5 in Figure 5) and the actual measurement (measurement 6 in Figure 5). Then the allowed interval for the measurements is set to the calculated mean value plus the allowed variation range as presented in Table 10. To pass the soft condition check, the value of all measurements in the test period array and the actual measurement must be within this allowed interval. If a measurement does not meet all the soft conditions, the test period array is not completely emptied, but only the first measurement (Measurement 1 in Figure 5) is removed. Then the mean value of the

modified test period array (measurements 2 to 5 in Figure 5) and the actual measurement is determined and the check for soft conditions is repeated with this new mean value. This process is repeated until the actual measurement passes the check. In the worst case, the test period array becomes completely emptied. Then the actual measurement, which has already passed the hard conditions check, also passes the soft conditions check as the mean value of single measurement is equal to the value of the measurement and so automatically lies within the allowed variation range. TCC.m proceeds then with the hard condition check for the next measurement in the production data file.

1.10. Efficiency calculation (EffCalc.m)

The result of the check on test condition described in the previous section is the matrix *datapoints* that contain pointers to valid test periods in meanmatrix. Figure 6 shows an example of a part of *meanmatrix* that contains a valid test period. At this point the efficiency for a test period can be calculated. The product of mass flow, heat capacity of the heat transfer fluid and the temperature difference between collector inlet and outlet is integrated with respect to time to calculate the useful energy gain of the collector. The global solar irradiance upon the aperture plane of the collector measured by the pyranometer is integrated over time and multiplied with the gross collector area to quantify the energy incident upon the collector during the data period. The ratio of the two calculated values represents the thermal efficiency of the collector. It is important to mention that the integration interval contains only the data period, not the pre-data period. The calculated efficiency is plotted with respect to the related temperature difference-irradiance ratio in °C per W/m^2. The temperature difference is the average inlet temperature minus the average ambient temperature.

No	ΔT	$\dot{m}$	c_p	$t_{f,e}$	$t_{f,i}$	G_t	
1	1.1	2.3	4.1	70	59	800	Pre-data period
2	1.11	2.31	4.1	71	60	801	
…	…	…	…	…	…	…	
n-d	1.09	2.3	4.1	70	59	804	Data period
…	…	…	…	…	…	…	
n-1	1.1	2.29	4.1	71	61	808	
n	1.12	2.32	4.1	72	60	810	

Calculation of Thermal Efficiency

$$\eta_g = \frac{\int_{T_1}^{T_2} \dot{m} c_p (t_{f,e} - t_{f,i}) dT}{A_g \int_{T_1}^{T_2} G_t dT} = \frac{\sum_{k=n-d}^{n} \left(\dot{m} c_p (t_{f,e} - t_{f,i}) \Delta T \right)_k}{A_g \sum_{k=n-d}^{n} G_t \Delta T}$$

Calculation of temperature difference irradiance ratio

$$x = \frac{\sum_{k=n-d}^{n} \left((t_{f,e} - t_{f,i}) \Delta T \right)_k}{\sum_{k=n-d}^{n} \Delta T}$$

The results are generated!

datapoint = $\left(x, \eta_g \right)$

Figure 6 Computation of thermal efficiency and temperature difference irradiance ratio

1.11. Matrix results

The result matrix *results* contain the following information:

Table 12 Variables in matrix results

Column number	Variable	Units
1	Day of year	days
2	Start time of data period (local time)	sec
3	Useful energy gain	kJ
4	Solar Irradiance energy	kJ

5	Efficiency	-
6	Average inlet temperature	°F
7	Average ambient temperature	°F
8	Average solar irradiance	W/m^2
9	Temperature-irradiance ratio	$°C/(W/m^2)$
10	Start row predata period	row
11	Start row data period	row
12	Stop row test period	row
13	Average interval	rows
14	Deviation from solar noon, morning negative, afternoon positive	min

1.12. Symmetry to solar noon

One of the test conditions required that has not yet been discussed is symmetry to solar noon. For each inlet temperature level, two measurements shall be taken before solar noon and two after solar noon. According to the Standard, this procedure is intended to avoid any kind of transient effects that could bias the test results (ASHRAE Standard 93-2003, section 8.3.3.2). However, it would seem that the procedure is really intended to minimize incidence angle effects.

The check for symmetry is done manually in this version of the software. Two data points are symmetric if one is before and the other one is after solar noon and their deviations from solar noon differ by no more than 15 minutes. However, this value is not defined in the ASHRAE 93-2003 standard but chosen arbitrarily.

1.13. Conclusion

The software TestAnalyzer will be intensively tested during the next weeks to ensure that all of its components work properly. Also another module will be added that generates a final report as required by the ASHRAE Standard 93-2003.

2. Results of the first collector tests

2.1. Introduction

TestAnalyzer has been used to analyze the data of all thermal efficiency tests performed at MATC thus far. The original data have been averaged over intervals of 10 measurements, which corresponds to a time interval of approximately 10 seconds. The test condition check has found 18 valid data points. A total of 10 out of these 18 data points are symmetric to solar noon. To meet the ASHRAE Standard 93-2003 requirements, 6 more data points symmetric to solar noon are required. Thus, the results presented below are not in conformance with ASHRAE Standard 93-2003. However, they do provide a good indication whether or not the test facility and the data analysis procedures are yielding reasonable test results.

2.2. Results

Figure 7 shows the efficiency curve of the collector based on 10 data points. These data points contain five pairs which are symmetric to solar noon as described in Chapter 1.12. Two different methods have been used to fit a linear curve to the data points. The green line has been created using the standard technique of a least-squares fit. This method is prescribed by the ASHRAE Standard 93-2003 in Chapter 8.5. For the red curve the linear fit with bivariate regression has been used. Figure 7 shows that both methods lead to almost identical curves.

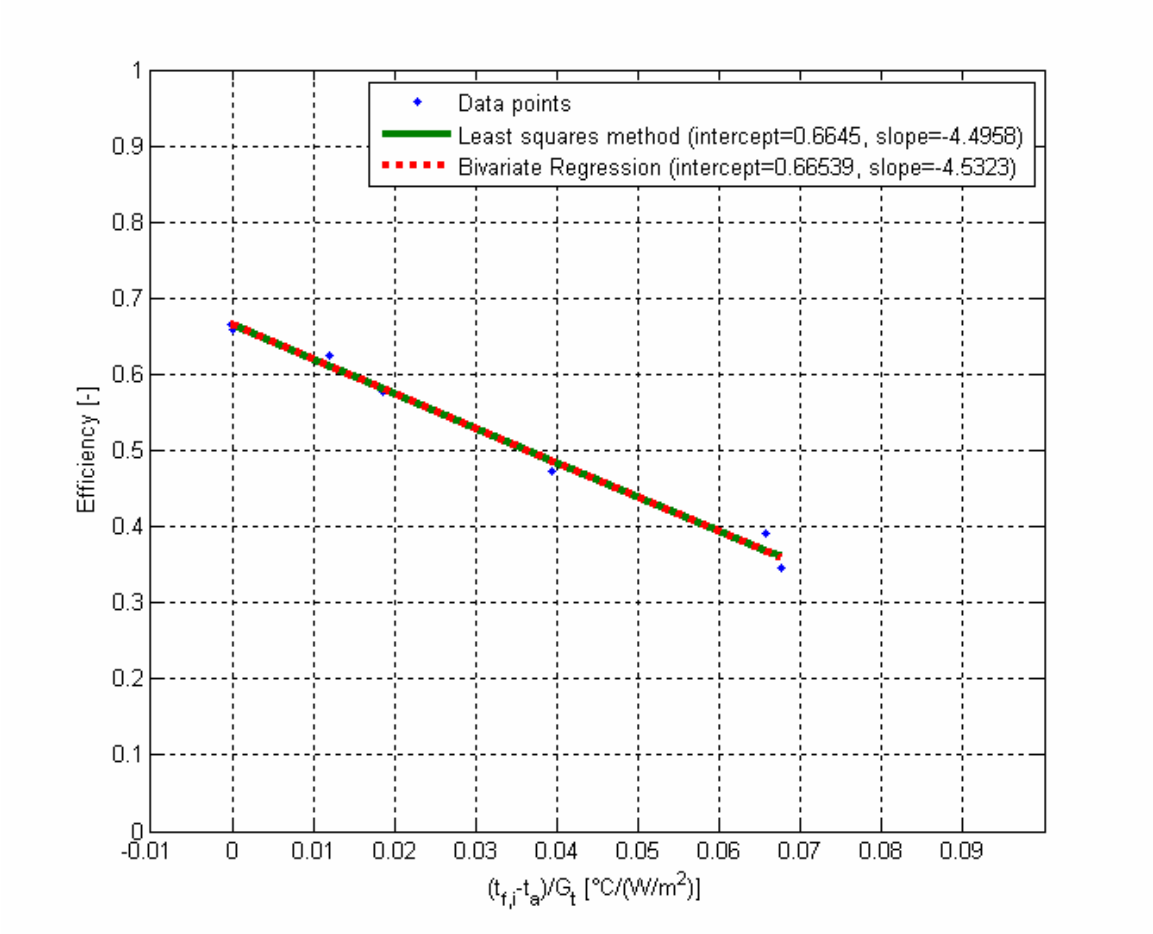

Figure 7 Collector test results, 10 data points symmetric to solar noon

Figure 8 contains the same information as Figure 7, but instead of using only the 10 symmetric data points, all 18 data points are used. This time the curves based on different method for fitting the data differ. According to the linear least squares method dictated in the Standard, the intercept is at 64.6 % efficiency with a slope of -4.15 while the bivariate regression methods results in an intercept of 67.3% efficiency and a slope of -4.88.

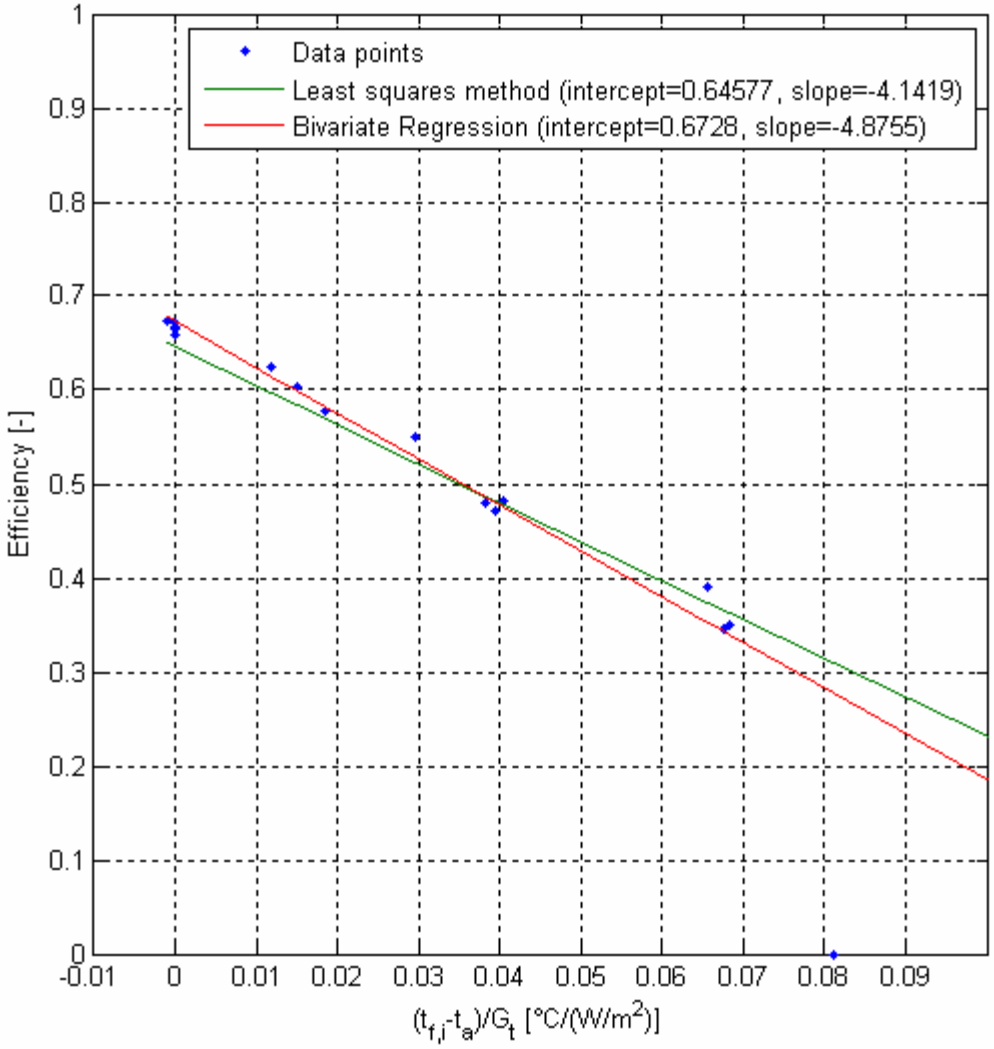

Figure 8 Collector test results, 18 data points, not symmetric to solar noon

2.3. Conclusion

The results presented above are typical for flat plate collectors of the type tested at MATC. This results show that the test facility at MATC does have the capability to provide reasonable test data.

Applying another fitting method than that one required by ASHRAE Standard 93-2003 can result in different results for the same data points, as Figure 8 shows.

3. Quality of total radiation measurements

3.1. Introduction

The total radiation on a horizontal surface is required for the analysis of the collector test data. This value can be measured directly with a horizontal pyranometer (direct method) or it can be calculated from beam radiation measured by a sun tracking pyrheliometer and the diffuse radiation measured by a horizontal pyranometer with a sun tracking shading disc (combined method). The objective of this section is to evaluate the accuracy of the two methods. In case there is a difference in quality between the two methods, the method with higher quality will be chosen. The first step is to compare results of the direct and the combined method, based on real measurements.

3.2. Calculations

The total solar irradiance on a horizontal plane I, the total diffuse radiation on a horizontal plane I_d and the beam radiation normal to the sun I_{bn} are measured on the roof of the University of Wisconsin-Madison's Engineering Research Building in Madison and published as data files for each day of the year by the ISIS data monitoring project[3].

The total radiation measurements have larger uncertainty for large values of the solar zenith angle. The total radiation is measured on a horizontal surface so that at times near sunrise and sunset, the incidence angle upon the pyranometer plane is close to 90 degree. While the diffuse part of the total radiation should be measured nearly independently of the zenith angle, the beam part is expected to be measured to low for values close to 90 degree. However, the direct beam radiation is measured separately by a sun tracking pyrheliometer and the diffuse radiation by a horizontal pyranometer with a shading disc. Based on the two latter measurements the value for the total radiation will be calculated and compared to the pyranometer-measured value. The difference between measured and calculated values of total radiation will be called "error" in the following.

The three radiation variables I_{bn}, I_d, and I are related according to Equations (1.4) and (1.5).

$$I_b = I_{bn}\cos(\beta) \tag{1.6}$$

$$I = I_b + I_d \tag{1.7}$$

I_{bn} is the beam radiation on a surface normal to the sun. Figure 3 shows that the tilt angle β of a surface normal to the sun is always equal to the solar zenith angle θ_z. So β is given by Equation (1.3). Solar zenith angle values are provided within the ISIS data files.

[3] Integrated Surface Irradiance Study (ISIS) Network, http://www.srrb.noaa.gov/isis/index.html

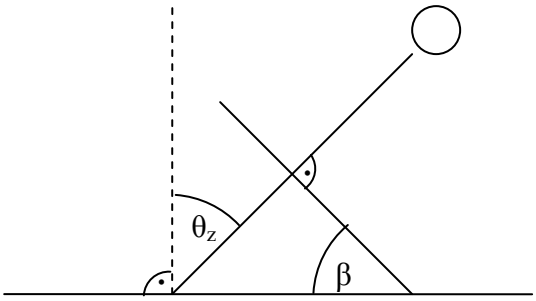

Figure 9 Tilt angle of a surface orientated normal to beam radiation

$$\beta = \theta_z \tag{1.8}$$

As a result of the shown dependency, the measured values of beam and diffuse radiation can be used to check the measured values of total radiation. Assuming that the measurements of beam and diffuse radiation are correct, the absolute and relative errors of the total radiation measurements can be calculated. This is done by calculating the total radiation with Equation (1.5), the absolute error with Equation (1.9), and the relative error with Equation (1.10).

$$absolute\_error = I_{measured} - I_{calculated} \tag{1.9}$$

$$relative\_error = \frac{I_{measured} - I_{calculated}}{I_{calculated}} \tag{1.10}$$

3.3. Results

The ISIS radiation data and the relative error with respect to the solar zenith angle have been plotted for four days in 2006, two clear days and two overcast days. For both kinds of weather one day before ISIS performed sensor calibration on Jul 13, 2006, and one day after the calibration has been chosen.

The ISIS irradiance plots for each pair of days are followed by a plot which compares the absolute and relative error before and after calibration. Finally, the uncertainty of the absolute error (due to uncertainty in zenith angle, beam, and diffuse radiation measurements) has been calculated and plotted for both days.

3.3.1. Clear days

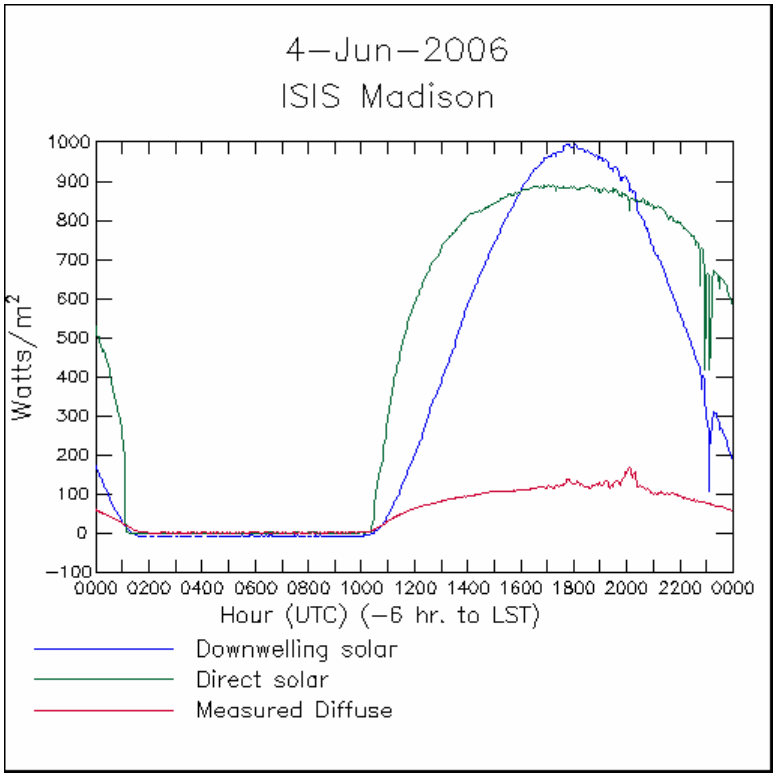

Figure 10 ISIS irradiance plot, clear day, before calibration

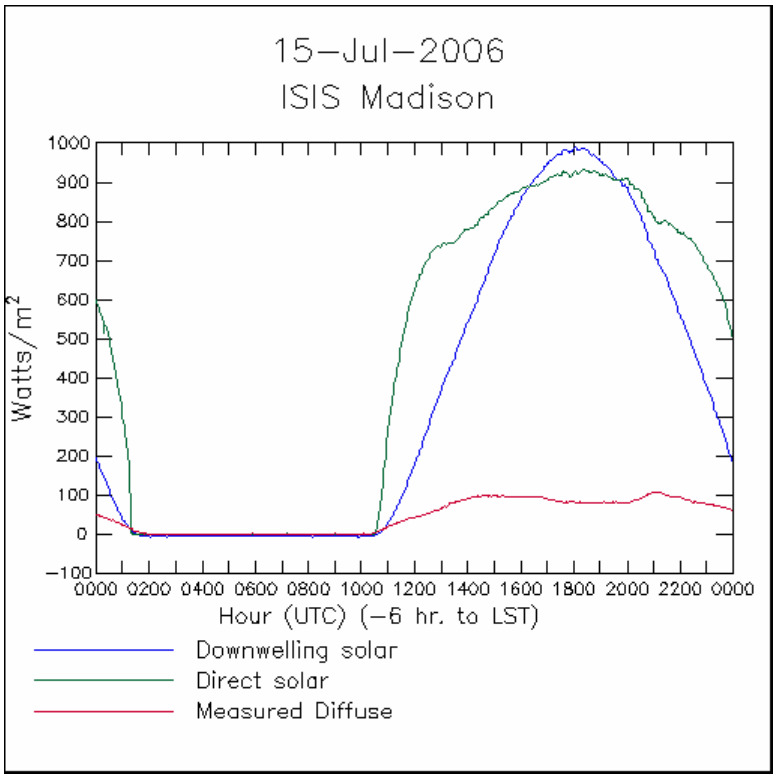

Figure 11 ISIS irradiance plot, clear day, after calibration

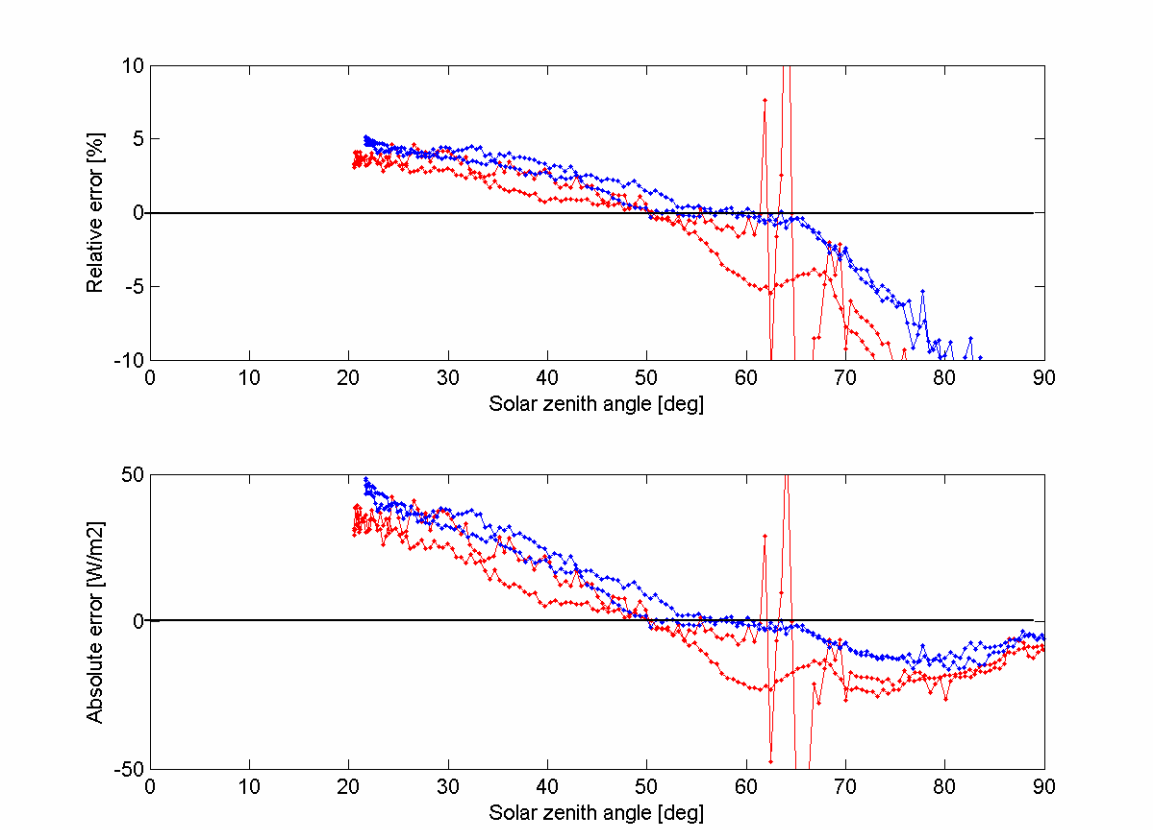

Figure 12 Relative and absolute error of measured and calculated total irradiance; clear day; red before calibration (Jun 4, 2006), blue after calibration (Jul 15, 2006)

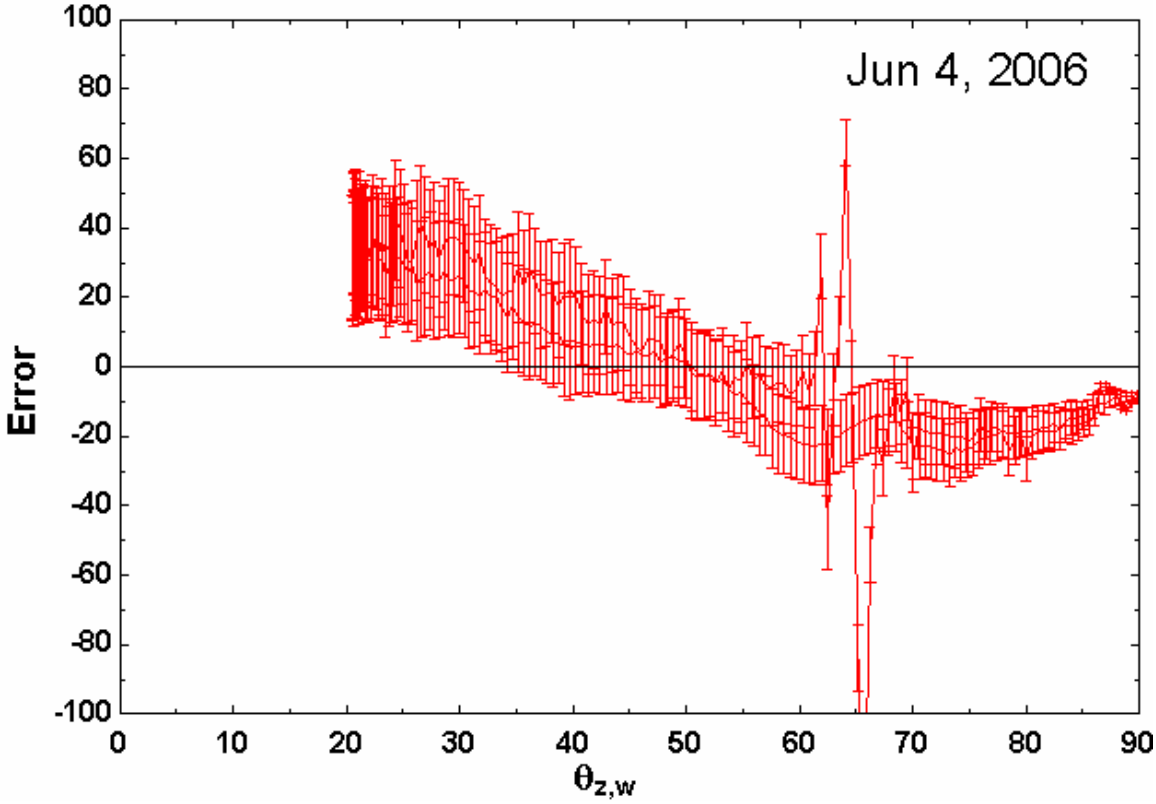

Figure 13 Uncertainty of absolute error, clear day, before calibration

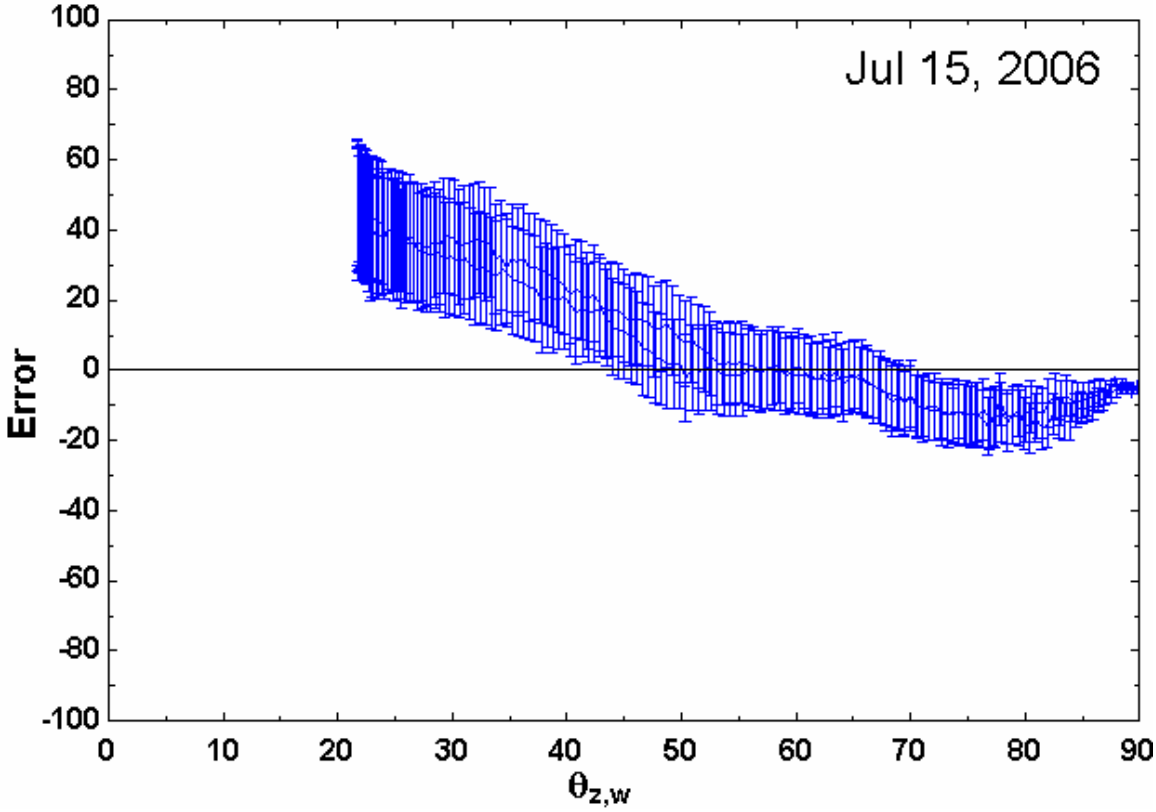

Figure 14 Uncertainty of absolute error, clear day, after calibration

3.3.2. Overcast days

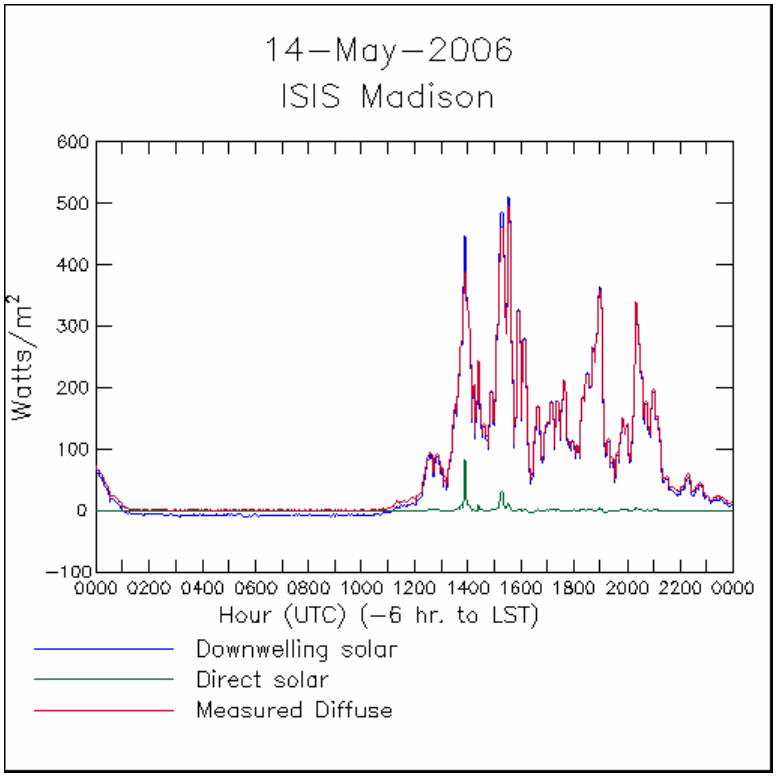

Figure 15 ISIS irradiance plot, overcast day, before calibration

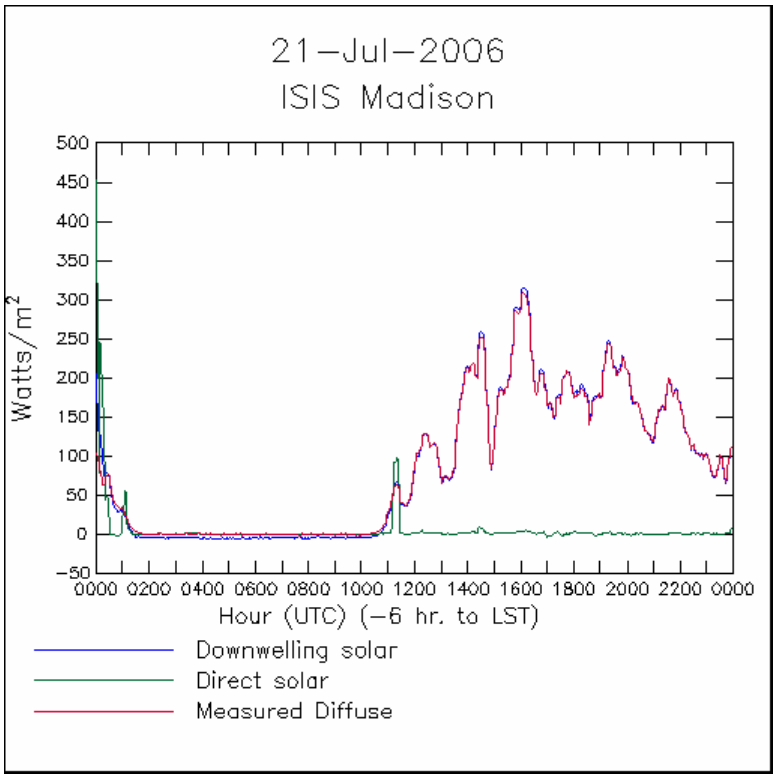

Figure 16 ISIS irradiance plot, overcast day, after calibration

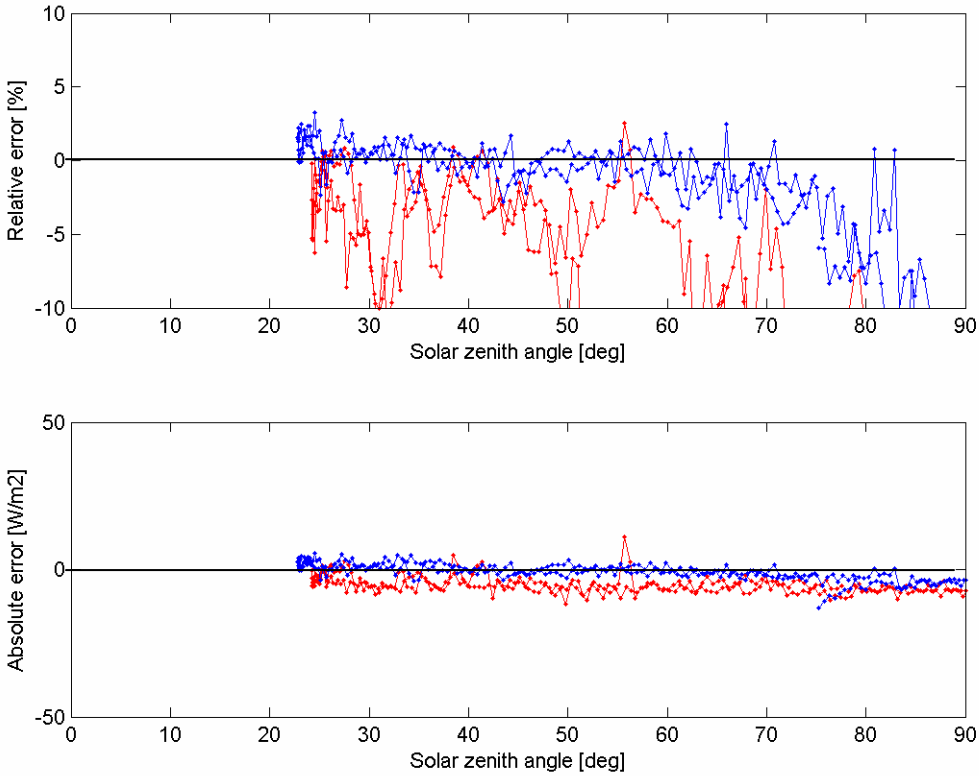

Figure 17 Relative and absolute error of measured and calculated total irradiance; clear day; red before calibration (May 14, 2006), blue after calibration (Jul 21, 2006)

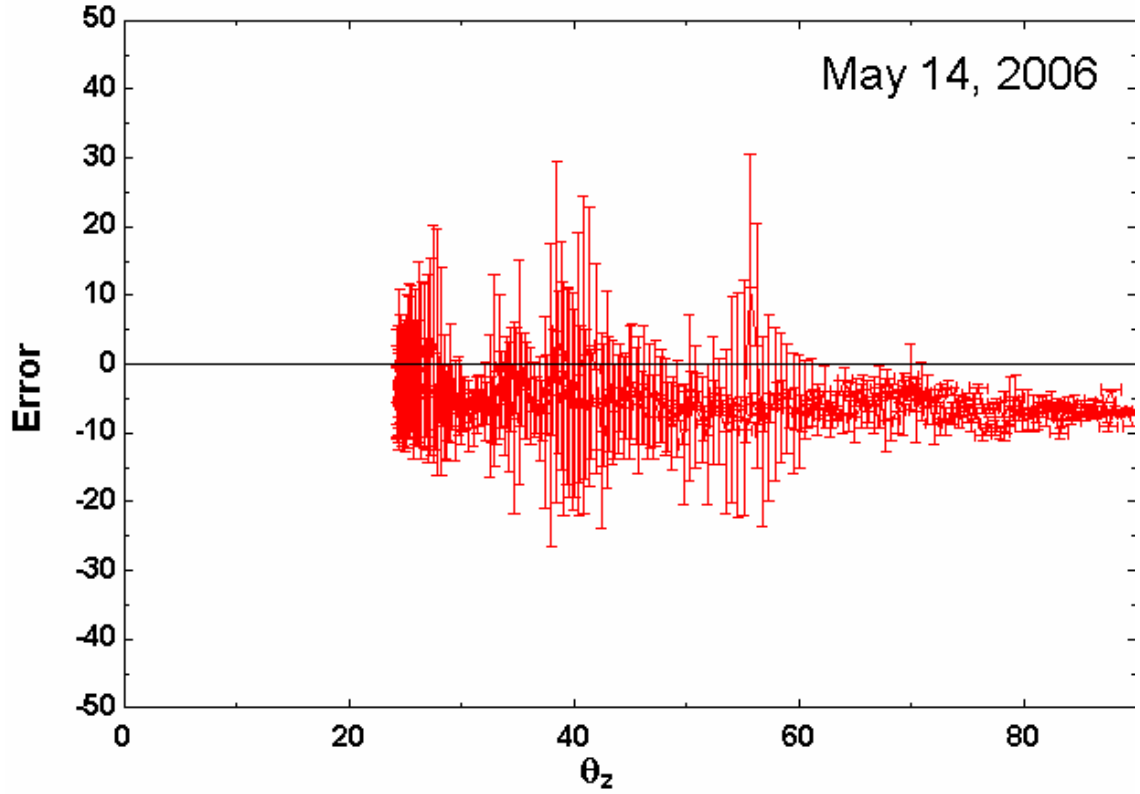

Figure 18 Uncertainty of absolute error, overcast day, before calibration

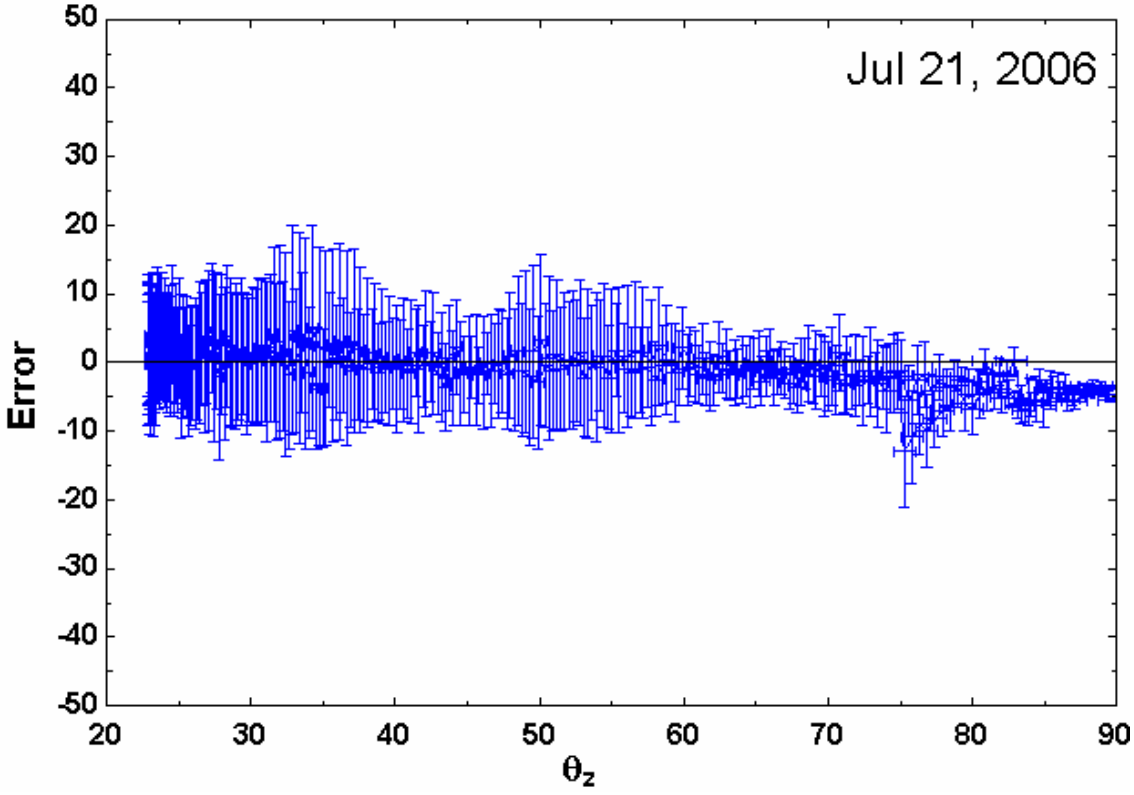

Figure 19 Uncertainty of absolute error, overcast day, after calibration

3.4. Discussion

For solar zenith angle greater than 80 degrees, the relative error is greater than 10% for all considered days - as expected.

Looking at the uncertainty plot for July 15 (Figure 11), the difference between measured and calculated total irradiance seems to be small in the range from 50 to 65 degree zenith angle, but for smaller zenith angles (20 - 50 degree) calculations and measurements do not agree, even with consideration of uncertainty, as shown in Figure 14. Three possible reasons are:

1. The beam radiation measurements are inaccurate for 20-50 degrees.
2. The total radiation measurements are inaccurate for 20-50 degrees.
3. The diffuse radiation measurements are inaccurate for 20-50 degrees.

The diffuse and total radiation measurements agree very well on overcast days as shown in Figure 17. The absolute and relative errors on Jul 21, 2006 (after calibration) do not show the tendency to higher errors for lower zenith angles in the range between 20 and 50 degrees. On this day, the beam radiation is measured to be nearly zero, so the beam radiation measurement cannot affect the error. Consequently the measurement of beam radiation by the pyrheliometer or, as a fraction of total radiation, by the pyranometer must cause the errors.

3.5. Conclusion

The results presented above have shown that direct measurements of total radiation with a pyranometer do not lead to the same results as the combined measurements of direct normal and diffuse radiation with the current instruments. The analysis of the test results leads to the conclusion that the measurement of beam radiation causes the deviation in values for total radiation between direct and combined method. The pyrheliometer measures only the beam radiation while the pyranometer measures the total radiation which includes beam and diffuse radiation. From the results presented above it can not be derived whether the pyrheliometer or the pyranometer measures the beam radiation more accurate.

At this point John Augustine of the National Oceanic & Atmospheric Administration (NOAA) has provided help and suggestions. He is responsible for ISIS program and is therefore involved in solar radiation measurements. The question which of the two instruments and therefore which of the two methods is more accurate has already been analyzed. Michaelsky et al. (1999) have shown that the combined method using beam and diffuse measurements is more accurate than the direct measurement of total radiation with a pyranometer[4]. Two major errors reduce the accuracy of the pyranometer measurements, the cosine error and the temperature offset. Figure 12 shows the cosine error of the pyranometer. Figure 17 shows the temperature offset, which was reduced by the calibration of the pyranometer. The cosine error occurs only if beam radiation is

[4] Michalsky et al. (1999) Optimal Measurement of Surface Shortwave Irradiance Using Current Instrumentation, J. Atmos. and Ocean Tech., 16, 55-69

present. Consequently, the measurement of diffuse radiation by a pyranometer does not exhibit the cosine error. This conclusion agrees with the results presented above.

For the described reasons the combined method will be used for determining the total radiation whenever possible. A pyranometer is used to measure the irradiance upon the collector during the tests. This measurement is very important as it significantly affects the test results. As a fixed test mount is used during the tests, the incidence angle upon the pyranometer changes. It will be analyzed in how far the cosine error reduces the quality of the test results.

.

4. Pyranometer calibration

A Precision Spectral Pyranometer, model PSP, manufactured by The Eppley Laboratory, Inc., is installed at the MATC collector test mount to measure the total irradiance upon the collector aperture plane. The MATC PSP has been calibrated by the manufacturer.

As the test analysis is based not only on the measurements of the MATC PSP but also on ISIS radiation measurements, it is desirable to check in how far the MATC and ISIS measurements agree with each other. For this purpose the MATC PSP has been orientated horizontally facing the sky to measure total solar irradiance on a horizontal surface. The results have been compared to ISIS measurements. Two methods have been used to receive total radiation from ISIS data. The direct method uses the measurements of a single pyranometer (total radiation on horizontal surface is measured directly) while the combined method combines the separate measurements of beam radiation and diffuse radiation. The calculations required for the latter method are the same as described in Section 3.2 of this report. The MATC measurements have been averaged over the same 3 minutes periods as the provided ISIS data to allow comparison.

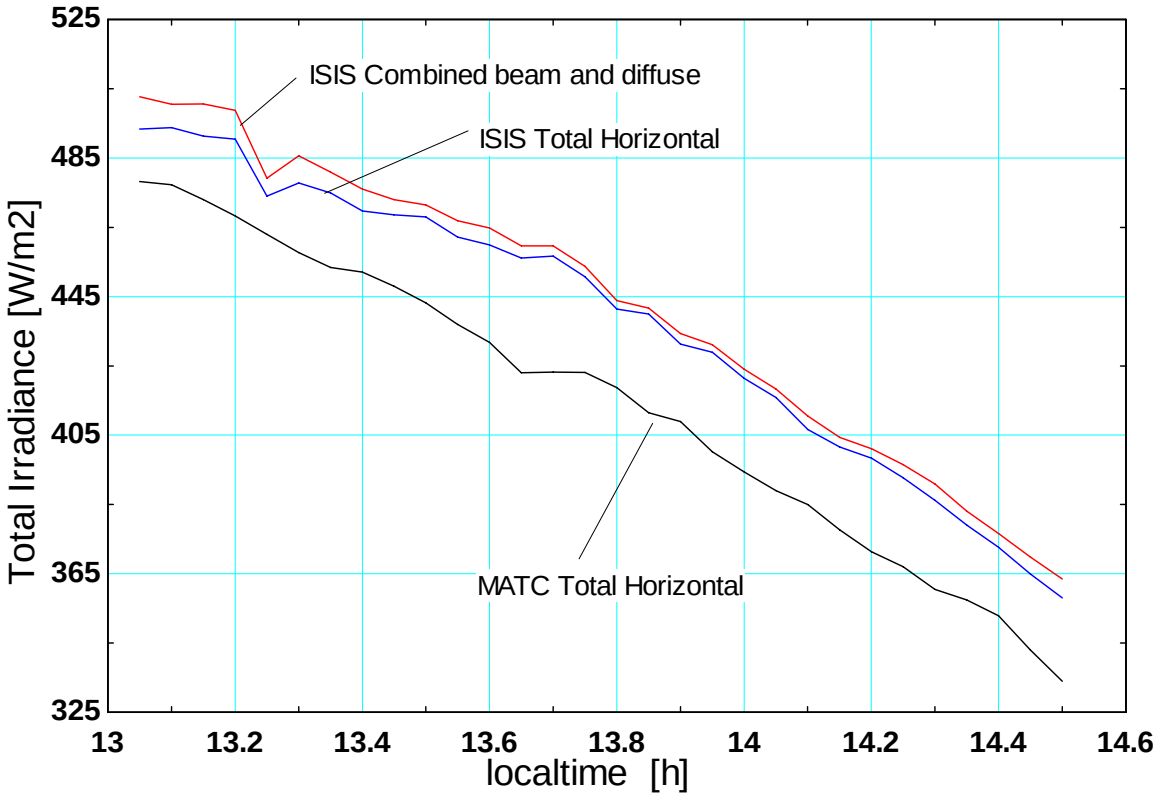

Figure 20 Irradiance measurements from MATC and ISIS

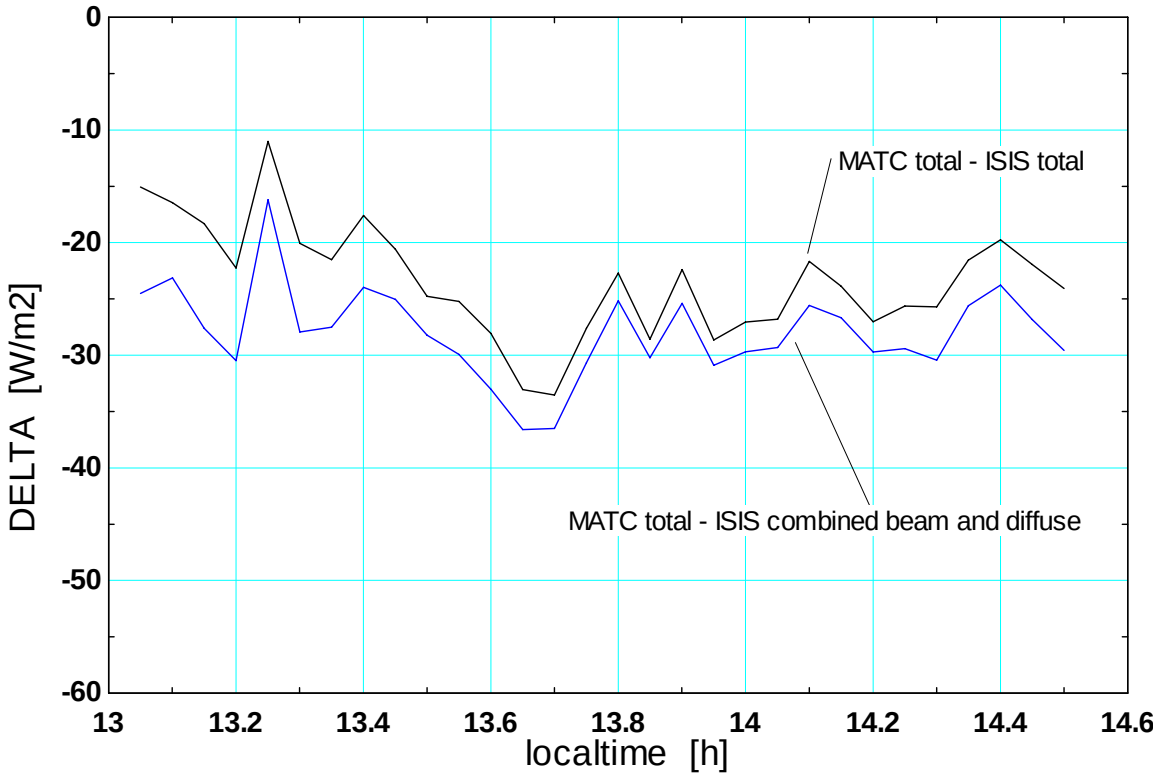

Figure 21 Absolute deviation of the MATC pyranometer compared to ISIS pyranometer (1, black) and ISIS beam and diffuse (2, blue)

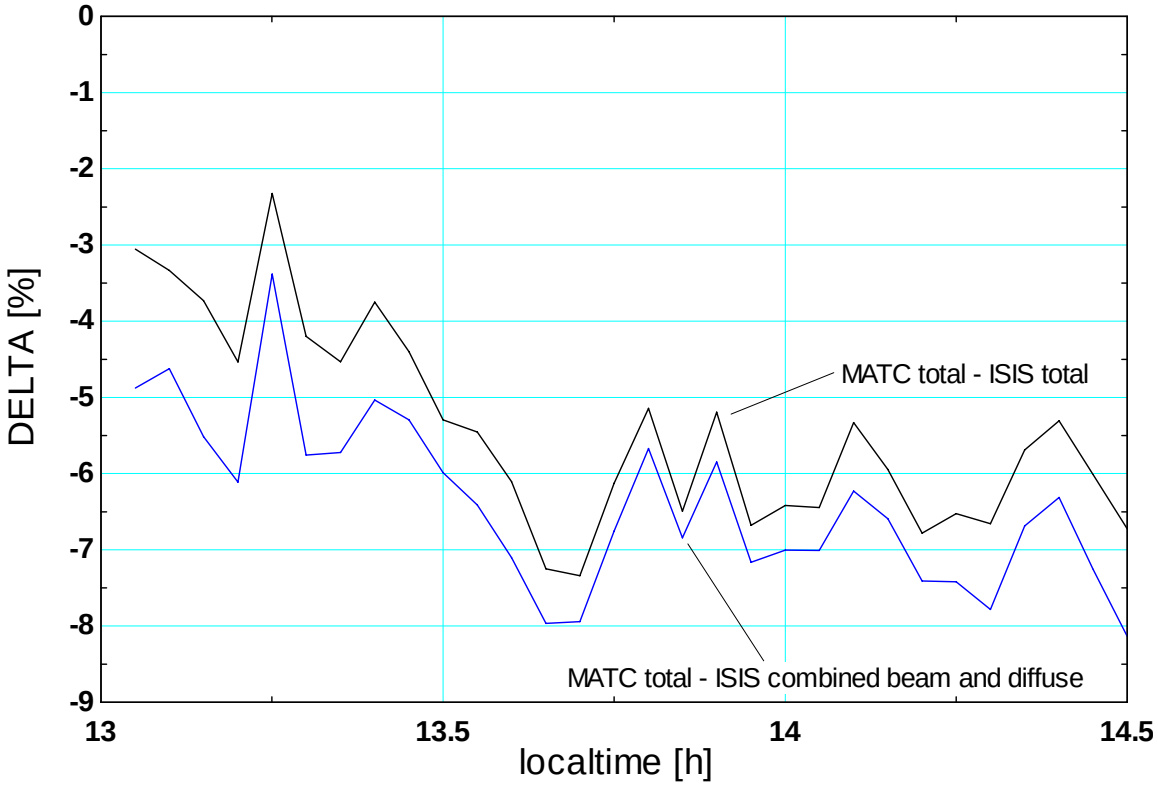

Figure 22 Relative deviation of the MATC pyranometer compared to ISIS pyranometer (1, black) and ISIS beam and diffuse (2, blue)

The data were taken on Jan 25, 2007. The MATC measurements have been performed at the test site where usually the collector test mount is positioned. The pyranometer has been placed on an elevated position two meters above ground, as shown in Figure 25 through Figure 27. The ISIS instruments are positioned on the roof of the ERB building in Madison. The linear distance between the two locations is about 8.3 kilometers.

Figure 20 show that the MATC and ISIS total radiation measurements have the same gradient on slightly different levels. So, as expected, the distance between the two locations is negligible on clear days like the one considered.

The MATC pyranometer measures the total irradiance to be 23.4 W/m^2 or 5.4% (on average) less than the measurements of the ISIS pyranometer. The deviation from the total irradiance calculated from ISIS beam and diffuse measurements is even greater, MATC measurements are on average 28 W/m2 or 6.4% below ISIS measurements.

A difference in the order of 8% is significant. Many factors can influence the measurements, like reflections of the surroundings, unclean instruments, etc. The question is whether the MATC or the ISIS are closer to the true total irradiance value, or whether both measurements are good and the actual irradiance differs at both locations.

5. Experimental Determination of the Ground Reflectance at the MATC Collector Test Site

5.1. Description of the experiment

The total solar irradiance upon a point 2 meters above the ground (A in Figure 23) can be divided into two fractions. The first one is irradiance coming from the sky I_{sky} (B in Figure 23), the second one irradiance coming from the ground I_{ground} (C in Figure 23).

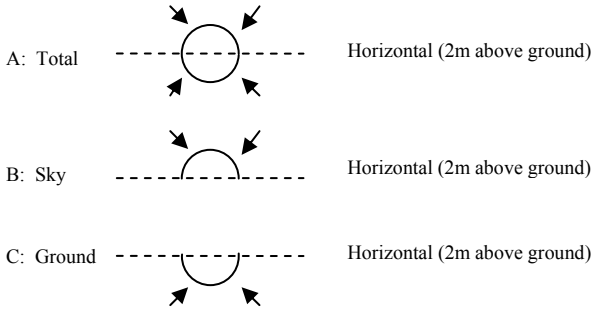

Figure 23 The different origins of irradiance

The ground reflectance ρ_g is the ratio of the ground irradiance and the total irradiance as shown in Equation (1.11).

$$\rho_g = \frac{I_{ground}}{I_{ground} + I_{sky}} \tag{1.11}$$

To determine the ground reflectance at the MATC collector test facility, the irradiance from the sky and the irradiance from the ground have been measured with the test setup shown in Figure 24. Only one pyranometer has been used. The sky and ground irradiance have been measured over two successive periods of 6 minutes. This sequence has been repeated three times before and three times after solar noon.

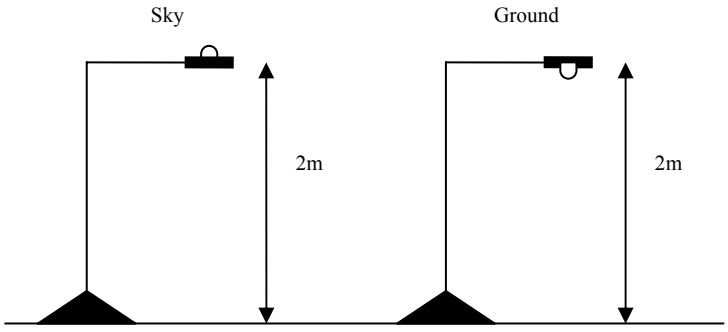

Figure 24 Test setup for ground reflectance determination

The test was performed on Jan 25, 2007. The ground at the test site was partly covered with snow, as shown in Figure 25. The test has been performed at the same position the collector test mount is placed during the collector tests. The irradiance measurements have been averaged over a 5 minutes interval within the 6 minute test periods. The one minute difference allows excepting measurements during turning the pyranometer.

5.2. Pictures

Figure 25 Total radiation on horizontal measurements, picture in direction south-east, ground partly snow covered, © Thomas Kaminski

Figure 26 Total radiation on horizontal measurements, picture in direction north-west, showing closest building, © Thomas Kaminski

Figure 27 Total radiation on horizontal measurements, picture of pyranometer and measure showing height above ground, © Thomas Kaminski

5.3. Results

The results are presented in Table 13. The first column contains the start time of the test period and the orientation of the pyranometer. The second column shows the averaged irradiance. The third column contains the calculated ground reflectance based on the irradiance in the same row and the preceding row.

Table 13 Ground reflectance results on Jan 25, 2007

Test period start time	Orientation	Average irradiance [W/m^2]	Ground reflectance
11:48:45	up	491.2	
11:54:20	down	125.5	0.20
12:00:32	up	511.9	0.20
12:05:49	down	132.5	0.21
12:11:19	up	475.2	0.22
12:18:35	down	112.8	0.19
Average			**0.20**

The ground reflectance was found to be 0.2 for the partly snow covered ground. This value is below the expected typical range from 0.3 to 0.7. Additional tests will be conducted to on a day with no snow cover and on a day with full snow cover to show the range of ground reflectance at the test site.

6. Literature list

The technical literature relating to collector testing is rich. The first results of a literature research are presented below. This literature will be used to support the further development of the solar collector test facility at MATC and to identify possible modifications of the ASHRAE Standard 93-2003. The table does not necessarily list the titles of the references, but the relevant contents concerning collector testing.

6.1. Collector Test Standards

ASHRAE Standard 96	Unglazed, flat-plate, liquid collectors	1989
ASHRAE Standard 93-2003	All other collectors	2003
EN 12975-1	General requirements	2000
EN 12975-2	Test methods	2001
ISO 209806-1	Glazed liquid collectors	1994
ISO 209806-2	Reliability testing	1995
ISO 209806-3	Unglazed collectors	1996
CSA-F378-87	Canadian test standard for all kinds of collectors	1998
SRCC RM-1	Test Methods and Minimum Standards for Certifying Solar Collectors	1994
SRCC Document OG-100-05	Operating guidelines for certifying solar collectors	2005
SRCC Standard OG-100	Test Methods and Minimum Standards for Certifying Solar Collectors	2005

6.2. Test Results

SRCC	2004	Directory of solar collector ratings (OG-100)
SPF	2004	Solar collector test reports (Switzerland)
SRCC	2006	Directory of solar collector ratings (OG-100)
SRCC	2006	Summary of solar collector (OG-100) and water heating system ratings (OG-300)

6.3. Literature

Hayward	1979	Construction of a solar collector test facility
Beghi	1981	Experiences and recommendations for testing (liquid)
Beghi	1981	Experiences and recommendations for testing (liquid, short version)
Proctor	1984	A generalized method for testing all classes of collectors - II - Collector thermal constants
Proctor	1984	A generalized method for testing all classes of collectors - II - Collector thermal constants
Proctor	1984	A generalized method for testing all classes of collectors - III - Linearized efficiency equations
Kaminga	1984	Dynamic test method with Fourier transformation
Bourges	1991-1	Accuracy of European "all day test" - Part 1: Measurement errors
Bourges	1991-2	Accuracy of European "all day test" - Part 2: Prediction long term performance

Amer	1997	Comparison of dynamic test methods
Michalsky	1999	Problems of measuring total radiation with a single pyranometer
Dutton	2001	Temperature offset errors of pyranometers
Sabatelli	2001	Uncertainty analysis of ISO 9806-1
Li	2003	Uncertainty analysis of ISO 9806-1
Fischer	2003	The quasi-dynamic test method in EN 12975-2
Hou	2004	Time constant without inlet temp = ambient temp
Drück	2004	Background information about collector tests performed by Stiftung Warentest in Germany
Kratzenberg	2005	Comparison of the uncertainty of steady state test (ISO 9806) with quasi-dynamic test (EN 12975)
Facao	2006	Uncertainty analysis of steady state collector test method (provides also good overview of similar papers)

[1] *ANSI/ASHRAE Standard 93-2003, Methods of Testing to Determine the Thermal Performance of Solar collectors.* ISSN 1041-2336, ASHRAE, Inc., 2003, 1791 Tullie Circle, Ne, Atlanta, GA30329